THE JOURNAL OF PHYSICAL CHEMISTRY A
A JOURNAL OF THE AMERICAN CHEMICAL SOCIETY

pubs.acs.org/JPCA

Article

$\pi\sigma^*$-Mediated Nonadiabatic Tunneling Dynamics of Thiophenols in S_1: The Semiclassical Approaches

Published as part of The Journal of Physical Chemistry virtual special issue "Paul L. Houston Festschrift".

Junggil Kim, Kyung Chul Woo, Kuk Ki Kim, and Sang Kyu Kim*

Cite This: *J. Phys. Chem. A* 2022, 126, 9594−9604

Read Online

ACCESS | Metrics & More | Article Recommendations | Supporting Information

ABSTRACT: The S−H bond tunneling predissociation dynamics of thiophenol and its *ortho*-substituted derivatives (2-fluorothiophenol, 2-methoxythiophenol, and 2-chlorothiophenol) in S_1 ($\pi\pi^*$) where the H atom tunneling is mediated by the nearby S_2 ($\pi\sigma^*$) state (which is repulsive along the S−H bond extension coordinate) have been investigated in a state-specific way using the picosecond time-resolved pump−probe spectroscopy for the jet-cooled molecules. The effects of the specific vibrational mode excitations and the SH/SD substitutions on the S−H(D) bond rupture tunneling dynamics have been interrogated, giving deep insights into the multidimensional aspects of the S_1/S_2 conical intersection, which also shapes the underlying adiabatic tunneling potential energy surfaces (PESs). The semiclassical tunneling rate calculations based on the Wentzel−Kramers−Brillouin (WKB) approximation or Zhu−Nakamura (ZN) theory have been carried out based on the ab initio PESs calculated in the (one, two, or three) reduced dimensions to be compared with the experiment. Though the quantitative experimental results could not be reproduced satisfactorily by the present calculations, the qualitative trends among different molecules in terms of the behavior of the tunneling rate versus the (adiabatic) barrier height or the number of PES dimensions could be rationalized. Most interestingly, the H/D kinetic isotope effect observed in the tunneling rate could be much better explained by the ZN theory compared to the WKB approximation, indicating that the nonadiabatic coupling matrix elements should be invoked for understanding the tunneling dynamics taking place in the proximity of the conical intersection.

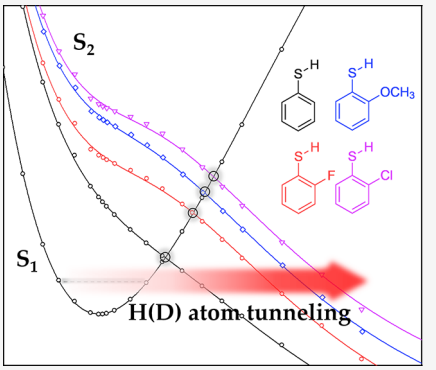

INTRODUCTION

Nonadiabatic dynamics is ubiquitous especially in the photochemical and/or photobiological processes where the closely spaced electronically excited states are heavily involved in the chemical reactions and/or structural transformation. Close-lying electronic states are then degenerate at some nuclear configurations, giving the multidimensional conical intersections where the Born−Oppenheimer approximation breaks down. Thereafter, the nonadiabatic transition especially in the proximity of the conical intersection occurs with the significantly high probability to govern the overall dynamic outputs such as reaction rates, product yields, branching ratios, or energy disposals.[1−4] The nonadiabatic transition probability is extremely sensitive to the nature of the reactive flux with respect to the electronic/nuclear configurations at the conical intersection, and thus its theoretical prediction (or the explanation of the experiment) has been quite challenging especially for polyatomic molecular systems. In this aspect, the $\pi\sigma^*$-mediated photochemistry of the heteroaromatic molecular system[5−9] has provided the nice platform for many recent years not only for elucidating the mechanism of the ultrafast nonradiative transitions frequently found in biological building blocks but also for the thorough understanding of the conical intersection dynamics.[10−14] Among the systems of interest, predissociation dynamics of thioanisole is particularly notable.[15−21] Therein, the S_1/S_2 and S_0/S_2 conical intersections are encountered along the S−CH_3 bond extension coordinate. The former is close to the vertical transition region whereas the latter is located at the later stage of the reaction. Due to the small energy difference (~3000 cm^{-1}) of two final distinct product channels into either $C_6H_5S\cdot(\tilde{A})$ or $C_6H_5S\cdot(\tilde{X})$,[22] the nonadiabatic transition probability could be precisely estimated from the analysis of product translational energy distributions in a state-specific way. The nonadiabatic dynamics from the well-defined quantum state of the reactant to that of the product gives the resonance-like features in the nonadiabatic transition probability, giving the unprecedented deep insights into the structural and dynamic properties of the

Received: August 16, 2022
Revised: December 2, 2022
Published: December 19, 2022

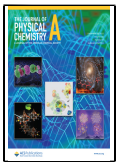

https://doi.org/10.1021/acs.jpca.2c05861
J. Phys. Chem. A 2022, 126, 9594−9604

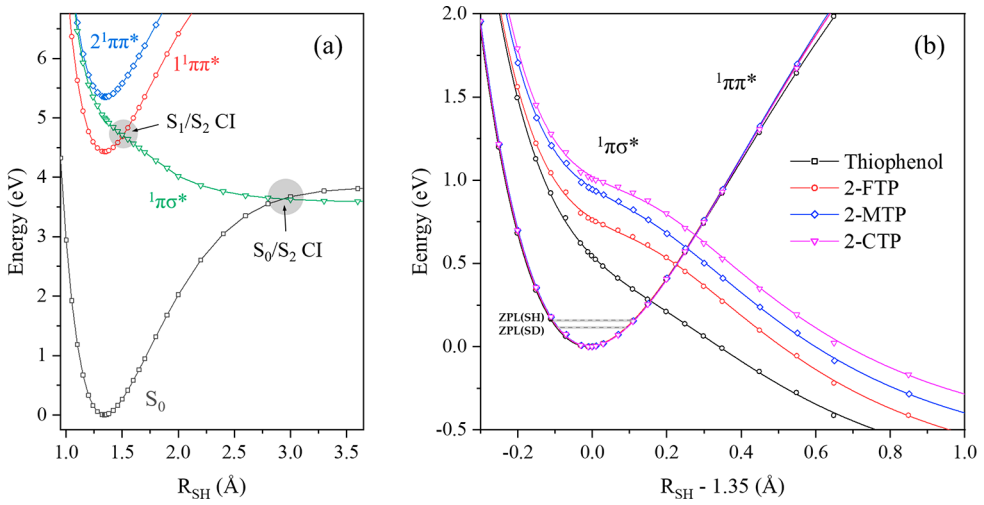

Figure 1. (a) One-dimensional potential energy curves of thiophenol for the four lowest singlet electronic states (S_0, $1^1\pi\pi^*$, $^1\pi\sigma^*$, and $2^1\pi\pi^*$) along the S−H bond extension coordinate. Two planar conical intersections associated with the S_2 ($\pi\sigma^*$) state are depicted in gray. (b) Potential energy curves of thiophenol (black square), 2-FTP (red circle), 2-MTP (blue diamond), and 2-CTP (purple triangle) corresponding to the $^1\pi\pi^*$ or $^1\pi\sigma^*$ states near the S_1/S_2 conical intersection calculated at the planar geometry. All rigid-body calculations have been performed using the CASPT2//SA4-CASSCF method at the frozen ground state equilibrium geometries except the S−H bond lengths. ZPL(SH) and ZPL(SD) stand for the zero-point energy level of thiophenol and thiophenol-*d*, respectively.

conical intersections responsible for the eventual S−CH_3 bond breakage.[15,17,21] It has also been found that the reactive flux in S_1 is bifurcated at the first $S_1(\pi\pi^*)/S_2(\pi\sigma^*)$ conical intersection into either the Herzberg type-I (electronic) or type-II (vibrational) predissociation process[23−25] with distinct reaction rates and nonadiabatic transition probabilities.[18] Very interestingly, the reactive flux of the type-I electronic predissociation is faster to give the higher nonadiabatic transition probability compared to the case of the type-II vibrational predissociation, indicating that the electronic predissociation in which the reactive flux should funnel through the rather narrow conical intersection region fast exhibits the higher nonadiabatic transition probability. Resonance-like enhancements of the nonadiabatic transition probability observed at the particular S_1 vibronic modes then provide the crucial information regarding the multidimensional nuclear configuration of the S_1/S_2 conical intersection, though they are rather limited to the Franck−Condon window.[21]

The overall characteristics of the potential energy surfaces in terms of curve crossings among three lowest singlet states (S_0, S_1, and S_2) are identical for thioanisole and thiophenol (including their chemical derivatives) (Figure 1). And yet, the mechanisms of the S-CH_3 or S−H bond dissociation are quite different from each other in many aspects. Namely, the S−CH_3 bond breakage of thioanisole takes place rather slowly with the S_1 lifetime (τ) of hundreds of picoseconds[18,26] whereas the S−H bond dissociation of the S_1 thiophenol occurs extremely fast to give $\tau \sim 50$ fs.[27−29] Moreover, the quantum-mechanical tunneling occurs very efficiently in the latter, whereas its probability is expected to be very low for the former presumably because of the much heavier reduced-mass in the fragmentation event. The S−H chemical bond dissociation of thiophenol (or its chemical analogues) thus provides the great opportunity to investigate the dynamic influence of the conical intersection on the tunneling dynamics as the tunneling barrier is shaped by the upper-lying conical intersection characterized along the multidimensional coordinates.[28,30−32] Notably, the O−H bond dissociation of the S_1 phenol, as a prototypical system of the $\pi\sigma^*$-mediated photochemistry, has been intensively investigated for many years. The upper limit of the O−H tunneling rate of the S_1 phenol at the zero-point level (ZPL) has been measured to give $\tau \sim 2.3$ ns.[33−36] This is more than $\sim 10^4$ times slower than that of the S−H bond rupture of the S_1 thiophenol at ZPL, indicating that the tunneling barrier height of the S_1 thiophenol should be much lower compared to that of phenol. This also implies that the S−H tunneling dissociation of thiophenol (S_1) would be largely influenced by the upper-lying S_1/S_2 conical intersection responsible for the shaping of the underlying adiabatic tunneling barrier, as it is located much closer to the S_1 minimum compared to the case of phenol. In this aspect, we focus (although the O−H tunneling dynamics of phenol and its analogs[36−40] have also been found to be extremely interesting) on the study of the S−H (or S−D) dissociation dynamics of the S_1 thiophenol or its chemical derivatives in terms of the mode specificity and the kinetic isotope effect as it may unravel the detailed dynamic influence of the conical intersection on the tunneling reactions.

It should be noted that the S−H(D) tunneling dynamics has recently been studied by our own group for several chemical derivatives of thiophenol including 2-fluorothiophenol (2-FTP), 2-methoxythiophenol (2-MTP), or 2-chlorothiphenol (2-CTP),[32,41−43] giving the very interesting dynamic features in terms of the mode-specific tunneling rates.[32] In the *ortho*-substituted thiophenol, the S_2 ($\pi\sigma^*$) state is found to be energetically lifted up with respect to the S_1 ($\pi\pi^*$) state in the vertical excitation region, giving the resultant tunneling barrier height that is much higher than that of the bare thiophenol along the S−H(D) bond extension coordinate.[41,42] The upper bound of the tunneling barrier in the one-dimensional picture has been roughly estimated from the S_1/S_2 curve-crossing at the planar molecular configuration to be 1800, 3900, 4400, or 5200 cm^{-1} for thiophenol, 2-FTP, 2-MTP, or 2-CTP, respectively (Figure 1). Although these barrier heights are most likely overestimated as the upper bounds of the adiabatic tunneling barrier, the qualitative trend of the experiment is rationalized as the S_1 lifetime at ZPL has been experimentally estimated to give $\tau \sim 0.05$, ~12, ~44, or ~230 ps for thiophenol, 2-FTP, 2-MTP, or 2-CTP, respectively, conform-

https://doi.org/10.1021/acs.jpca.2c05861
J. Phys. Chem. A 2022, 126, 9594−9604

ing to the general conception of the slower tunneling rate with the larger barrier height. Incidentally, it should be noted that the S_1 vibronic bands, which were nontrivial to be identified in thiophenol due to its ultrashort lifetime, could be well resolved now in 2-FTP, 2-MTP, or 2-CTP, giving the great opportunity to unravel the mode-specific tunneling behavior.[32] For instance, the tunneling rate is found to be increased by ∼2 times (compared to that at ZPL) at the two quanta of C−C−S−H out-of-plane torsional mode (τ_{SH}^2) excitation for all of 2-FTP, 2-MTP, and 2-CTP. This fact already indicates that the reactive flux spread along the C−C−S−H out-of-plane torsional coordinate would experience the much lowered effective tunneling barrier as it is shaped by the upper-lying multidimensional S_1/S_2 conical intersection along the derivative coupling vector on the conical intersection branching plane, for instance.[44]

Herein, we report the tunneling dynamics of the S_1*ortho*-substituted thiophenols (2-FTP, 2-MTP, and 2-CTP) in terms of their mode-dependent tunneling rates and H/D kinetic isotope effects (KIEs). The picosecond (or femtosecond) time-resolved pump−probe spectroscopy for the jet-cooled molecules has been employed for the state-specific lifetime measurements as well as their isotope effects. The calculations using the semiclassical tunneling theories have been carried out for the rational explanation of the experiment. It is particularly noteworthy that the KIE may be one of the most crucial factors for judging the validity of the theoretical models of tunneling. And yet, it seriously lacks the experimental result of the state-specific KIE of tunneling dynamics for the isolated chemical system to date. In this aspect, the state- and isotope-specific tunneling rates of thiophenols here provide the quite rare opportunity for the stringent test of the theoretical models of tunneling. Two semiclassical calculations based on the Wentzel−Kramers−Brillouin (WKB) approximation and the Zhu−Nakamura (ZN) theory have been carried out to be compared with the experiment. It is interesting to note that the tunneling rate calculated by the WKB approximation on the one-dimensional adiabatic potential energy curve already gives the quite good estimation of the experimental value within 1 order of magnitude. Furthermore, the significant increase of the tunneling rate upon the τ_{SH}^2 mode excitation could be well explained by the extension of the PES into the additional dimension along the C−C−S−H torsional angle coordinate. On the other hand, the H/D KIE has been found to be much better explained by the calculation based on the ZN theory compared to that with WKB, suggesting that the nonadiabatic coupling matrix elements imposed by the upper-lying conical intersection should be properly taken into account in the tunneling dynamic calculations.

METHODS

The samples of thiophenol and 2-FTP (98%, TCI) were heated to 40−60 °C in a stainless-steel reservoir and mixed with the neon carrier gas at the total pressure of ∼2.4 bar. The mixture was expanded into a high-vacuum chamber through a nozzle orifice (ϕ = 100 μm) of the Even−Lavie pulsed valve operating at the repetition rate of 200 Hz. The molecular beam was collimated by a 2 mm diameter skimmer and crossed by the femtosecond or picosecond laser pulses in the perpendicular geometry. The parent ions generated by the laser pulses were accelerated in the conventional velocity-map ion electrodes[45] before they were detected by the Chevron-type microchannel plates (MCPs) coupled to a phosphor screen. The ion signals were obtained by integrating the photomultiplier tube (PMT) signals and recorded as a function of delay time between pump and probe laser pulses. The delay time was manipulated by a retroreflector placed on a 300 mm long linear translational stage. The femtosecond pulses (Δt ∼ 35 fs) were generated by a pair of optical parametric amplifier (OPA) units (TOPAS-prime, Light Conversion) pumped by a 1 kHz fundamental output (791 nm) of the femtosecond Ti:sapphire regenerative amplifier system. The picosecond laser pulses (ΔE ∼ 20 cm^{-1}, Δt ∼ 1.7 ps) were generated by two separate units of OPA (TOPAS-800 ps, Light Conversion) pumped by the fundamental output (791 nm) of the 1 kHz picosecond Ti:sapphire regenerative amplifier. Both femtosecond and picosecond amplifier systems were seeded by a 80 MHz femtosecond Ti:sapphire oscillator. The pump and probe pulses were collinearly aligned into the vacuum chamber to be overlapped with the molecular beam without using the focusing lens. The polarization axis of the linearly polarized probe laser pulse was kept at the magic angle (54.7°) with respect to that of the pump laser pulse. The intensity of the laser pulses were attenuated by a set of neutral density (ND) filters before entering the vacuum chamber.

The ground-state geometries of thiophenol, 2-FTP, 2-MTP, and 2-CTP were optimized using a state-averaged complete active space self-consistent field (SA-CASSCF) method with 6-311++G(2df,2pd) basis sets. The CAS(12,11) active space consists of 12 electrons and 11 orbitals: three pairs of π/π^* Hückel orbitals, a pair of σ/σ^* orbitals on the C−S bond, a pair of σ/σ^* orbitals on S−H bond, and one nonbonding orbital on the S atom. The one-dimensional potential energy curves for the four lowest singlet states along the S−H bond extension coordinate were calculated using the same level of theory of the single-state second-order perturbation (SS-CASPT2) correction for the appropriate dynamic correlations. All CASPT2 calculations were carried out with an imaginary level shift of 0.4 au. While scanning, all molecular parameters except the S−H bond length were kept frozen at the equilibrium ground state (C_s) geometry. All calculations were performed using the MOLPRO program suite version 2010.1.[46]

RESULTS AND DISCUSSION

A. State-Specific H(D)-Tunneling Rates of Thiophenols in S_1. The S_1 state lifetime (τ) of thiophenol had been previously estimated to be ∼50 fs from the homogeneously broadened spectral bandwidths in the photofragment excitation (PHOFEX) spectra obtained by monitoring the H fragment as a function of the excitation energy.[28] This experiment conforms to the femtosecond time-resolved transients taken at the S_1 ZPL (λ_{pump} ∼ 285.8 nm), Figure 2. Considering the cross-correlation width of ∼130 fs (the full width at half-maximum of the instrumental Gaussian function), the single exponential fit to the transient gives τ ∼ 70 fs for the S_1 ZPL of thiophenol. This is quite consistent with the previous femtosecond time-resolved measurement by the Longarte group.[29] The S_1 lifetime seems to be invariant with the increasing vibrational energy, indicating that the wavepacket may be swept away from S_1 too quickly to reveal any mode dependency. The KIE (k_H/k_D) is less pronounced, giving τ ∼ 82 fs for thiophenol-*d* (C_6H_5S-D). Actually, the KIE is maintained to be small in the 1.2−1.4 range in the whole explored S_1 internal energy range (see Table S1 in the Supporting Information). This exceptionally small KIE

https://doi.org/10.1021/acs.jpca.2c05861
J. Phys. Chem. A 2022, 126, 9594−9604

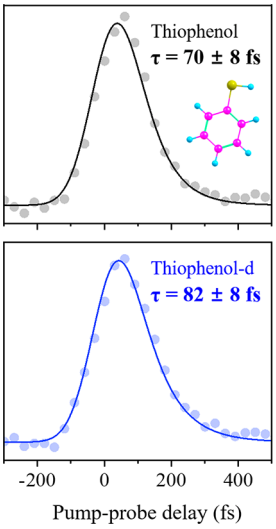

Figure 2. Femtosecond-resolved transients obtained at ZPL of thiophenol (upper trace) and thiophenol-*d* (lower trace) to give the S_1 lifetimes of ∼70 or ∼82 fs, respectively (see the text). The transients are fitted by the convolution of the single-exponential molecular response function convoluted with the instrumental Gaussian function.

suggests that the effective tunneling barrier may be extremely low for the S_1 thiophenol. The sharp variation of the anisotropy parameter observed in the angular distribution of the D fragment from the thiophenol-*d* indicates that the S_1/S_2 curve-crossing in the Franck−Condon window may be just ∼600 cm^{-1} above the S_1 ZPL,[28] giving still the upper limit of the tunneling barrier as the effective tunneling barrier might be significantly lower considering the existence of saddle points along the out-of-plane torsion coordinates.[44]

The substitution of the electronegative moiety on the *ortho*-position of thiophenol lifts up the energy gap between $\pi\pi^*$ and $\pi\sigma^*$ states quite substantially, resulting in the significant increase of the tunneling barrier height, Figure 1b. This happens to 2-FTP, 2-MTP, and 2-CTP. Accordingly, due to their lengthened S_1 lifetimes, many well-resolved S_1 vibronic states could be identified in the S_1-S_0 (nanosecond or picosecond) resonance-enhanced two-photon ionization (R2PI) spectra of *ortho*-substituted thiophenols,[32,41−43] unlike the case of thiophenol where the R2PI spectrum could not be obtainable.[27,28] And then, the picosecond time-resolved transient for each S_1 vibronic band is taken to give the lifetime corresponding to the state-specific tunneling rate. In addition to the previously reported lifetime measurements,[32] we have carried out further investigations here for the complete experimental data of the tunneling dynamics of the *ortho*-substituted thiophenols (2-FTP, 2-MTP, and 2-CTP) and their deuterated species (vide infra). For instance, the lifetime of 2-FTP-*d* has been newly estimated to be ∼278 ps at the S_1 ZPL (Figure 3), and this is ∼23 times slower compared to that of 2-FTP (∼12.3 ps). The KIE is maintained above ∼20 in the low S_1 internal energy (0−250 cm^{-1}) whereas it converges to ∼10 with increasing the energy. The dramatic KIE observed in 2-FTP and 2-FTP-*d* nicely demonstrates that the S−H(D) bond dissociation takes place via tunneling and the S_1-state dissipation should be mainly attributed to the tunneling process. The mode-dependent changes of the tunneling rates of 2-FTP and 2-FTP-*d* are interesting and should be further investigated in the near future. It is notable that the tunneling

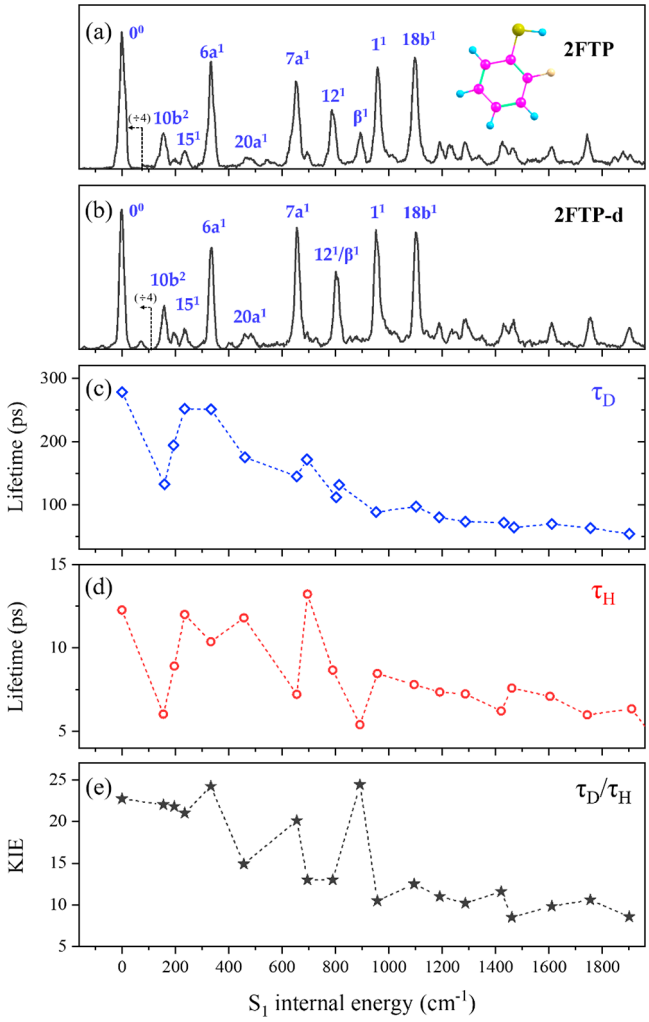

Figure 3. State-specific S_1 tunneling rates of 2-FTP and 2-FTP-*d*. Picosecond (1 + 1′) resonance-enhanced multiphoton ionization spectrum of (a) 2-FTP[32] and (b) 2-FTP-*d* obtained by monitoring the parent ion signal at the zero time delay between the pump and probe laser pulses. Vibronic assignments are adopted from refs 32 and 41. S_1 lifetimes of (c) 2-FTP-*d* (τ_D) and (d) 2-FTP (τ_H) obtained from the single-exponential molecular response function fits to the transients taken at individual vibronic levels. (e) State-specific KIEs determined from k_H/k_D ($=\tau_D/\tau_H$). The KIE values are plotted based on the energies of vibronic peaks of 2-FTP in (d).

rate is accelerated by twice to give τ ∼ 133 ps at the out-of-plane C−C−S−D torsional mode (τ_{SD}^2) excitation (159 cm^{-1}) whereas it is slowed down again by increasing the S_1 internal energy to give τ ∼ 194 ps ($10b^2$) or ∼252 ps (15^1) at 193 or 253 cm^{-1}, respectively, as similarly found in the mode-specific tunneling rates of 2-FTP (Figure 3). This experimental finding (equally found for 2-FTP and its deuterated analog) confirms that the adiabatic tunneling barrier is dynamically shaped by the upper-lying conical intersection, especially along the out-of-plane torsional coordinate, which is parallel to the derivative coupling vector on the S_1/S_2 conical intersection branching plane.[27,47,48] The mode-dependent fluctuation of the tunneling rate disappears as the S_1 internal energy increases above ∼1000 cm^{-1} for both 2-FTP and 2-FTP-*d*, whereas the lifetime converges to ∼5 or ∼50 ps at ∼2000 cm^{-1} for 2-FTP or 2-FTP-*d*, respectively. This may indicate that the given internal energy becomes rapidly randomized into the isoenergetic dark

https://doi.org/10.1021/acs.jpca.2c05861
J. Phys. Chem. A 2022, 126, 9594−9604

manifolds by the intramolecular vibrational redistribution (IVR) process starting from the internal energy of ~1000 cm^{-1}.[32] Such a mode randomization might be responsible for the fast tunneling rate as well as the decrease of KIE (k_H/k_D ~ 10) in the high internal energy region.

A number of well-resolved S_1 vibronic bands are also identified in the picosecond R2PI spectra of 2-MTP and 2-MTP-*d*.[32] The state-specific tunneling lifetimes measured at individual vibronic modes are shown in Figure 4. The lifetime

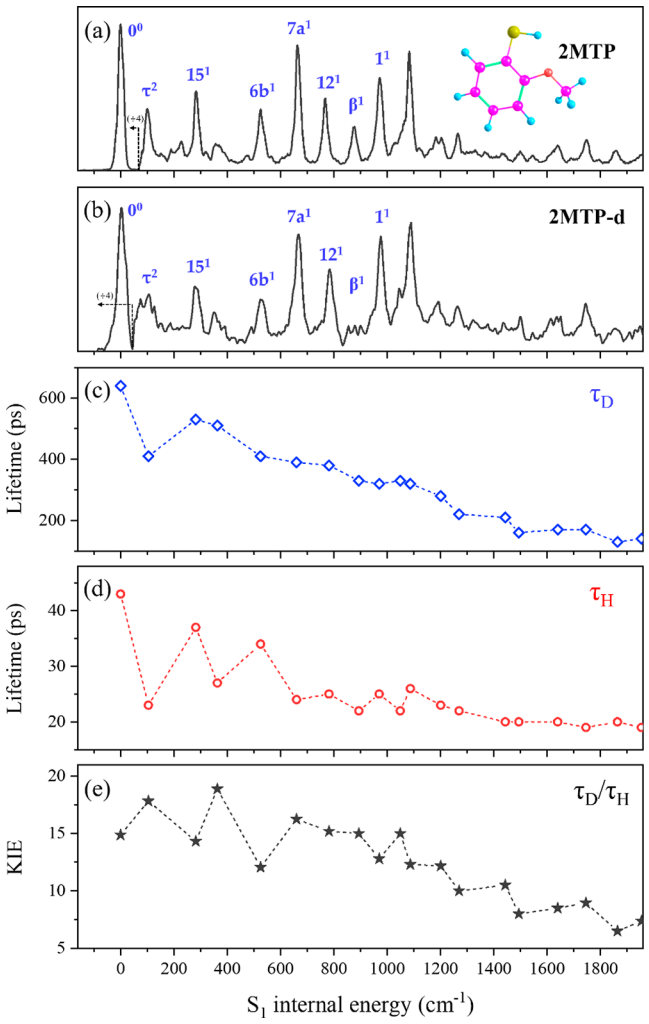

Figure 4. State-specific S_1 tunneling rates of 2-MTP and 2-MTP-*d*. Picosecond (1 + 1′) resonance-enhanced multiphoton ionization spectrum of (a) 2-MTP[32] and (b) 2-MTP-*d* with appropriate vibronic mode assignments adopted from refs 32 and 42. S_1 lifetimes of (c) 2-MTP-*d* (τ_D) and (d) 2-MTP (τ_H) obtained from the single-exponential molecular response function fits to the transients. (e) State-specific KIEs determined from k_H/k_D ($=\tau_D/\tau_H$). The KIE values are plotted based on the energies of vibronic peaks of 2-MTP in (d).

of the S_1 ZPL of 2-MTP or 2-MTP-*d* has been found to be ~44 or ~640 ps, respectively, giving the large KIE of ~15. Similar to the case of 2-FTP (or 2-FTP-*d*), the tunneling rate gets increased abruptly at the out-of-plane torsional mode (τ_{SH}^2 (τ_{SD}^2)) excitation at ~101 cm^{-1} (~104 cm^{-1}) to give τ ~ 23 ps (~410 ps) for 2-MTP (2-MTP-*d*). This experimental observation confirms again that the tunneling rate is expedited when the reactive flux is spread along the out-of-plane torsional angle along which the adiabatic tunneling barrier is dynamically shaped by the upper-lying S_1/S_2 conical intersection. It seems to be noteworthy that the KIE measured at the τ_{SH}^2 and τ_{SD}^2 mode excitations remains the same as that at ZPL, although the KIE is anticipated to be diminished with the increase of the tunneling rate in the adiabatic picture. This behavior has also been observed for 2-FTP and 2-FTP-*d* (Figure 3), suggesting that the conventional adiabatic model of the tunneling might not be appropriate for the description of tunneling in the proximal presence of the conical intersection where the nonadiabatic coupling could be highly influential (vide infra). With the increase of the S_1 internal energy, the lifetime of 2-MTP or 2-MTP-*d* converges to give τ ~ 20 or 150 ps at ~2000 cm^{-1}, respectively, giving the KIE of ~7. The decrease of KIE with increasing the S_1 internal energy could be the consequence of the interplay between IVR and tunneling in the presence of the strong intramolecular hydrogen bonding.[42] The multidimensional tunneling potential energy surfaces that are dynamically influenced by the upper-lying conical intersection should be invoked for the better understanding of the experiment (vide infra). It should be emphasized here that the relaxation pathway of the S_1 2-CTP is seemingly quite different from that of 2-FTP or 2-MTP.[32] The S_1 lifetime of ~230 ps found at the ZPL of 2-CTP, unlike other *ortho*-substituted thiophenols, is not entirely attributed to the S−H tunneling dissociation. Rather, the exceptionally fast non-adiabatic transition (e.g., internal conversion) contributes quite significantly to the S_1 state relaxation,[49,50] and thus the quantum yield of the S−H tunneling reaction could be much less than unity, as manifested in the S_1 lifetime of ~635 ps measured at the ZPL of 2-CTP-*d* (giving the extremely small KIE value of ~2.8). This is the strong evidence that the S_1 lifetime does not fully reflect the tunneling reaction. Actually, the photochemistry of 2-CTP seems to be completely different from that of 2-FTP or 2-MTP whereas it is extremely interesting at the same time, and thus it is subject to the further investigation as an independent subject.

B. Semiclassical (WKB or ZN) Tunneling Rate Calculations. The WKB approximation is intuitively well accepted, and thus it has been vastly employed for the explanation of the tunneling processes of many chemical systems.[33,34,39,51] Under the slowly varying tunneling potential (V) compared to the de Broglie wavelength of a particle, the WKB tunneling probability (P_{WKB}) is given as follows.

$$P_{WKB} = \exp\left\{-2\int_{x_1}^{x_2}\sqrt{\frac{2\mu}{\hbar^2}[V(x) - E]}\,dx\right\} \quad (1)$$

Here, μ is the reduced mass of the tunneling moiety (H or D), E is the internal energy of the system, and the one-dimensional tunneling potential energy curve (V) is confined by the classical turning points (x_1, x_2) along the tunneling coordinate (x). As the tunneling occurs along the S−H(D) bond extension coordinate, the tunneling lifetime is given by the following relation.

$$\tau = (\nu_{str}\cdot P_{WKB})^{-1} \quad (2)$$

Here, ν_{str} represents the vibrational frequency (Hz) associated with the S−H or S−D bond stretching mode approximately at ~2,550 or 1,850 cm^{-1}, respectively. Using the one-dimensional potential energy curve calculated at the CASPT2//SA4-CASSCF(12,11) level of theory (Figure 1b), the WKB lifetimes are calculated to be compared to the experimental results. It is quite remarkable that the WKB tunneling rate on

https://doi.org/10.1021/acs.jpca.2c05861
J. Phys. Chem. A 2022, 126, 9594−9604

Table 1. S_1-State Lifetimes Calculated at the ZPL of Thiophenol, 2-FTP, 2-MTP, or 2-CTP by Using the WKB Approximation or the ZN Theory (See the Text for Details)

		estimated lifetimes at the S_1 ZPL							
		thiophenol		2-FTP		2-MTP		2-CTP	
model		τ_H (ps)	τ_D (ps)	τ_H (ps)	τ_D (ps)	τ_H (ps)	τ_D (ps)	τ_H (ps)	τ_D (ps)
	experiment	**0.070**	**0.082**	**12.3**	**278**	**44.4**	**640**	**230**	**635**
WKB	1D	0.045	0.302	2.01	101	16.4	2390	130	53600
	2D w/ torsion (τ)	0.034	0.238	1.36	61.9	7.04	763	31.5	11900
	2D w/ bending (β)	0.044	0.270	1.93	93.2	15.2	2090	115	42400
	3D w/ τ and β	0.032	0.199	1.31	56.5	6.57	624	28.0	10400
ZN	2D w/ τ	**0.122**	**0.491**	**28.1**	**978**	**396**	**16300**	**397**	**9900**

the one-dimensional adiabatic PES already reproduces the experiment quite well within 1 order of magnitude, Table 1. For instance, the ultrashort lifetime of 70 fs (or 82 fs) of thiophenol (or thiophenol-*d*) at ZPL is predicted to be 45 fs (or 302 fs) by WKB. Overall, as listed in Table 1, the H atom tunneling rate is much overestimated by the WKB calculation at the given PESs, giving the much shorter tunneling lifetime compared to the experimental result. However, the tunneling rate of the D atom detachment is significantly underestimated by WKB, giving the much larger KIE compared to the experimental result. That is, the KIE of ∼6.7, ∼50, or ∼145 is predicted by the one-dimensional WKB calculation for thiophenol, 2-FTP, or 2-MTP, respectively, which are much larger than the respective experimental values of ∼1.2, ∼23, or ∼14 measured at ZPL (vide infra).

Though the WKB model is adiabatic in nature, the tunneling reaction of the polyatomic systems cannot be described by the one-dimensional PES. Accordingly, as the tunneling barrier is multidimensional in nature, the WKB calculations on the PES extended into the two or three-dimensional coordinates have been carried out. We have chosen the out-of-plane C−C−S−H(D) torsional or the in-plane C−S−H(D) bending coordinate as the additional dimension. The vibrational modes associated with these coordinates disappear when the H(D) atom detachment is complete, and thus those modes could be strongly coupled to the tunneling reaction coordinate as they may not belong to the spectator modes. It should be noted that the two-dimensional PES could not be smoothly scanned by the CASPT2 method due to the diverging issue in the vicinity of the conical intersection at the present time. Instead, the two-dimensional rigid-scanned "PT2-corrected" potential energy surfaces along the S−H bond extension and C−C−S-H torsional angle (ϕ) coordinates have been constructed by the scaling of the CASSCF potential surfaces to the level of CASPT2//SA4-CASSCF(12,11). Briefly, the two-dimensional PT2-corrected potential surfaces were constructed by multiplying the two-dimensional CASSCF potential surfaces by a linear scaling factor correcting the CASSCF values to the CASPT2 energies in the C_S symmetry constraint. It is noteworthy that the rigid scan of the potential energy surface along the C−S−H bending angle (θ) could be carried out at the CASPT2 level without the diverging issue, indicating that the C−S−H bending angle belongs to one of the seam coordinates of the conical intersection. The construction of the PT2-corrected PESs have been described in the Supporting Information.

In Figure 5, the one-dimensional cuts of the two-dimensional PT2-corrected potential surfaces are depicted near the S_1/S_2 conical intersection along the S−H extension coordinate at many different C−C−S−H torsional angles. In principle, the

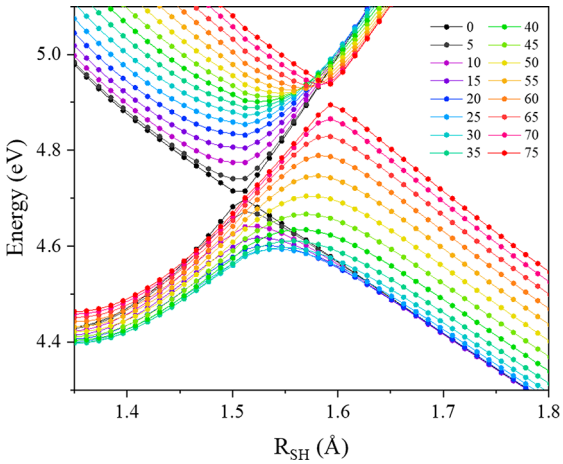

Figure 5. PT2-corrected potential energy curves of thiophenol along the S−H extension coordinate calculated at different C−C−S−H torsional angles (in degrees). The PESs obtained from the SA4-CASSCF(12,11) level of calculation are scaled by the CASPT2 energy values (see the text for details). All geometric parameters except the S−H bond length and C−C−S−H torsional angle are kept fixed at those of the ground state equilibrium geometry.

potential energy curve drawn at the torsional angle of 0° (planar) is exactly same as that obtained from the CASPT2 calculation (Figures 1 and 5). As a matter of fact, according to the PT2-corrected two-dimensional potential energy surfaces, the saddle point of the potential energy surfaces has been found at the C−C−S−H(D) dihedral angle of ∼28° at ∼0.12 eV below the S_1/S_2 conical intersection, giving the small but non-negligible tunneling barrier for the S−H(D) extension. This is quite consistent with the previous experiment[28] or the recent high-level calculations reported by Lin et al.[44] A tiny kinetic isotope effect found for thiophenol and thiophenol-*d*, however, may reflect the significant contribution of the alternative mechanism where the H(D) atom predissociation takes place on the barrierless potential energy surfaces that are developed along the branching plane of the conical intersection. The full-dimensional potential energy surfaces constructed by the more elaborated computational methods such as the multistate CASPT2 could be desirable for solving this puzzling issue in the near future.

The WKB tunneling probability has been calculated based on the one-dimensional potential energy curve projected from the two-dimensional PT2-corrected potential energy surfaces at the specific C−C−S−H torsional angle. The tunneling probability as a function of the torsional angle ($P_{WKB}(\phi)$) is then calculated at many different torsional angles, and it is analytically fit by the linear combination of multiple cosine

https://doi.org/10.1021/acs.jpca.2c05861
J. Phys. Chem. A 2022, 126, 9594−9604

functions. The S_1 state wave function as well as its probability distribution ($\psi^2(\phi)$) in the Franck−Condon region ($R_{SH} \sim 1.35$ Å) is numerically solved by diagonalizing the Hamiltonian matrix on the discrete variable representation (DVR) grids on the one-dimensional potential energy curve analytically fitted along the ϕ coordinate.[52] The effective tunneling probability at ZPL is then obtained by the weighted average of $P_{WKB}(\phi)$ according to $\psi^2(\phi)$ over the whole range of ϕ from −90° to +90°. The lifetime is then obtained by the equation in eq 2. For the WKB calculation on the PES extended along the C−S−H bending angle coordinate, the SQRT(*V*-*E*) term in eq 1 has been modified according to the calculated $V(\theta)$ at the conical intersection region (e.g., $R_{SH} \sim 1.51$ Å for thiophenol). As the C−S−H bending angle belongs to the conical intersection seam coordinate, its dynamic influence on tunneling is less significant. The details of the WKB calculations on the two- or three-dimensional potential energy surfaces are given in the Supporting Information.

The WKB tunneling lifetimes calculated on the two- or three-dimensional PESs are compared with the experimental results, Table 1. As anticipated, the WKB tunneling rate is predicted to be more than 2 times faster when the potential energy surfaces are extended into the out-of-plane torsional coordinate (it is quite notable that the tunneling rate is substantially influenced by extending the dimensionality of the potential energy surface even at the zero-point level), whereas it is only slightly accelerated by the extension into the C−S−H bending angle coordinate. The facilitated tunneling rate observed at the τ_{SH}^2 (τ_{SD}^2) mode excitation for 2-FTP (2-FTP-*d*) or 2-MTP (2-MTP-*d*) could also be rationalized nicely by the WKB calculation on the two-dimensional PES extended along the C−C−S−H torsional angle coordinate. Namely, the S_1 lifetime of 1.36 ps (or 7.04 ps) calculated at ZPL is predicted to be 0.72 ps (or 2.67 ps) at the τ_{SH}^2 mode excitation for 2-FTP (or 2-MTP) when $P_{WKB}(\phi)$ is weight-averaged for $\psi^2(\phi)$ calculated at two quanta of τ_{SH} mode. As mentioned above, the extension of PES into the dimension of the C−S−H bending angle coordinate gives the little influence on the tunneling rate (Table 1), implying that the multidimensionality of the potential energy surfaces with respect to the remaining (3*N*−8) seam coordinates of the conical intersection might not be very influential on the tunneling dynamics. The quantitative explanation of the experiment by the WKB method is not satisfactory, and yet it should be emphasized that the WKB tunneling rate is predicted to be much faster by the extension of the otherwise one-dimensional potential energy surfaces into two or three dimensions, strongly indicating that one should take into account the multidimensional tunneling barrier that is dynamically shaped by the upper-lying conical intersection. The WKB tunneling rate of thiophenol at ZPL on the three-dimensional potential energy surfaces, for example, is predicted to give $\tau = 32$ fs, which is shorter than the lifetime of 45 fs calculated on the one-dimensional PES. The KIE in terms of the qualitative trend is seemingly improved slightly by the extension of the dimensionality of PES, although it is still far from the experimental results.

As an alternative approach, we have employed the ZN theory to calculate the tunneling probability to take into account the nonadiabatic property of the tunneling process occurring in the vicinity of the S_1/S_2 conical intersection.[53−56] The ZN theory has been quite successful in describing the multistate curve-crossing problems (Landau−Zener nonadiabatic transition and/or nonadiabatic tunneling) for many years.[57−60] In the ZN theory, the nonadiabatic transition probability could be calculated on the adiabatic PESs without invoking the complicated adiabatic-to-diabatic transformation process. Instead, the nonadiabaticity has been taken into account from the topographic parameters associated with the PESs in the vicinity of the conical intersection. Here, the explicit solution of the ZN theory for the classically forbidden nonadiabatic tunneling has been employed for the case where two crossing potential energy curves have the gradients changing in the opposite directions along the tunneling coordinate. The tunneling probability by ZN (P_{ZN}) is then given as follows.

$$P_{ZN} = \frac{B(\sigma_c/\pi)\mathrm{e}^{-2\delta}}{[1 + (0.5\sqrt{a^2}/[\sqrt{a^2} + 1])B(\sigma_c/\pi)e^{-2\delta}]^2 + B(\sigma_c/\pi)\mathrm{e}^{-2\delta}} \quad (3)$$

Definitions of the parameters given in eq 3 are rather complex as described in a recent review article[56] though some critical ones are further discussed later. For the ZN tunneling probability calculations on the two-dimensional potential energy surfaces, we have employed the same strategy used for the WKB calculations (vide supra). Namely, P_{ZN} values calculated based on the one-dimensional PES projections at many particular C−C−S−H torsional angles are weight-averaged according to the probability of the S_1 ZPL wave function over the whole range of the torsional angle. It is quite notable that the ZN tunneling probability nearly vanishes at the planar geometry ($\angle$CCSH = 0°) where S_1 and S_2 do cross without the avoided-crossing, whereas the WKB tunneling probability is intrinsically insensitive to the nonadiabatic coupling at the conical intersection as expected. In Table 1, the ZN tunneling rates are calculated on the two-dimensional PT2-corrected PES extended along the out-of-plane torsional coordinate. Intriguingly, those are predicted to be slower than the experimental values this time within 1 order of magnitude. These are in the totally opposite side to the WKB calculations when the experimental values are in the middle. It seems to be too early to state that the ZN tunneling rates are substantially underestimated as the calculations have been carried out on the not-necessarily high-level ab initio PES in the much-reduced dimensionality. Considering the rational assumption that the use of the more exact multidimensional PES would give the faster tunneling rate, the ZN tunneling rate as the lower bound (slower than the experimental rate) might make more sense compared to the WKB tunneling rate as the upper bound (faster than the experimental rate) in the experiment.[30,61−63]

Quite intriguingly, it has been found that the KIE from the ZN tunneling rates gives the value to much closer the experimental one compared to the WKB calculation results, Table 1. For instance, KIE at the ZPL of thiophenol (2-FTP, 2-MTP) is predicted to be ∼4.0 (∼35, ∼41) from the ZN rates, which is much closer to the experimental value of ∼1.2 (∼23, ∼14) compared to the value of ∼6.2 (or ∼43, ∼95) predicted by the WKB calculation. However, it is quite apparent that the KIE is strongly influenced by the absolute tunneling barrier height value in the WKB calculation as the different zero-point energies of the H and D isotopologues bring the significant impact on the barrier-dependent behavior of the SQRT(*V*-*E*) term in eq 1. This implies that the overestimation of the KIE could be aroused from the overestimation of the calculated

https://doi.org/10.1021/acs.jpca.2c05861
J. Phys. Chem. A 2022, 126, 9594−9604

tunneling barrier height. In order to judge the validity of the semiclassical calculation methods, therefore, the calculated KIEs have been adjusted so that the absolute values of tunneling rates from two distinct calculations are equal to the experimental values (for undeuterated species) by manually manipulating the tunneling barrier height of the PESs. The (adjusted) KIEs calculated from WKB and ZN are now compared with the experimental values in Figure 6. The KIE

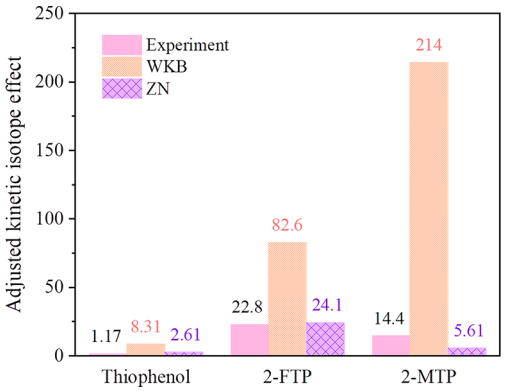

Figure 6. KIEs measured at the ZPL of thiophenol, 2-FTP, or 2-MTP from the experiment (magenta) are compared to the estimations from the semiclassical calculations (WKB, orange; ZN, purple). For the proper comparison, tunneling rates in the semiclassical calculations have been adjusted to the experimental values (see the text for details).

from WKB is much larger than the experimental value. Notably, the KIE from WKB shows the monotonic increase with the increase of the tunneling barrier height as expected from eq 1, giving KIE ~8.3, 83, or 214 for thiophenol (1800 cm^{-1}), 2-FTP (3900 cm^{-1}), or 2-MTP (4400 cm^{-1}), respectively. Remarkably though, the KIE from the ZN tunneling rates reproduces the experiment quite well, giving KIE ~ 2.6, ~24, or ~5.6 for thiophenol, 2-FTP, or 2-MTP, respectively. It is quite impressive that the KIE of 2-MTP is predicted to be smaller than that of 2-FTP by the ZN calculations (which conforms to the experiment) despite that the tunneling barrier height of the latter is higher than that of the former. This is completely opposite to the trend shown in the WKB calculation, indicating that the adiabatic description for the KIE in the tunneling reaction of thiophenols is insufficient. This is completely opposite to the trend shown in the WKB calculation, indicating that the nonadiabatic coupling terms as implemented in the ZN theory may have been manifested in the experimental KIE although it is subject to the more rigorous calculations in the near future.

The KIE is expected to be largely influenced by the zero-point energy difference between two isotopologues with respect to the S−H(D) tunneling coordinates within two classical bounds of the adiabatic tunneling barrier in the WKB formulation. This is intuitively correct in the adiabatic picture where the Born−Oppenheimer approximation holds. Namely, in the adiabatic picture, the role of the conical intersection is limited to the shaping of the low-lying adiabatic PES along the multidimensional degrees of freedom. In the ZN theory, on the other hand, two dimensionless parameters of a^2 and b^2 are additionally defined (eqs 3 and 4), representing the nonadiabatic coupling strength and the normalized internal energy of particle, respectively.[56] Those are given as follows.

$$a^2 = \frac{\hbar^2}{2\mu}\frac{\sqrt{F_1F_2}(F_1 - F_2)}{8V_{CI}^3} \qquad b^2 = (E - E_{CI})\frac{F_1 - F_2}{2\sqrt{F_1F_2}V_{CI}} \tag{4}$$

Here, F_i is the slope of the ith diabatic potential curve, E_{CI} is the energy of the avoided-crossing point, and V_{CI} is the diabatic coupling term. As a and b parameters (where the reduced mass (μ) and the ZPL difference are explicitly taken into account) reflect the geometric properties of two crossing diabatic potential surfaces, the ZN tunneling probability is anticipated to be strongly influenced by the nonadiabatic coupling terms.[53−56] Here, the adiabatic term (δ) is exactly same as the one used for the WKB tunneling probability (eqs 1 and 5).

$$\delta = \int_{x_1}^{x_2} \sqrt{\frac{2m}{\hbar^2}[V(x) - E]}\, dx \tag{5}$$

When the nonadiabatic coupling between upper and lower adiabats is negligible (or equally when the nonadiabatic term of a^2 vanishes), the ZN tunneling probability becomes identical to the WKB tunneling probability (eq 6).[56,64,65] This confirms that the nonadiabatic coupling at the conical intersection is fully invoked in the ZN tunneling rate whereas the WKB formulation is completely confined to the adiabatic picture.

$$P_{ZN,a\to 0} \cong e^{-2\delta} = \exp\left\{-2\int_a^b \sqrt{\frac{2m}{\hbar^2}[V(x) - E]}\, dx\right\} \tag{6}$$

In fact, the KIE of the tunneling reaction has been found to be strongly dependent on the adiabaticity of the system of interest and regarded to be quite useful for the judgment of the adiabaticity (or nonadiabaticity) of the chemical reactions under various circumstances.[66−72] In this regard, the fact that the KIE observed in thiophenol, 2-FTP, or 2-MTP is much better explained by the ZN theory indicates that the S−H(D) tunneling process should be nonadiabatic in nature. Namely, the tunneling is hardly described by the sole adiabatic picture for thiophenols, and the nonadiabatic coupling terms aroused by the close-lying conical intersection should be properly taken into account.

It is quite noteworthy that the importance of the nonadiabatic coupling terms in the $\pi\sigma^*$-mediated tunneling reactions of the heteroaromatic molecules has been emphasized in a series of computational studies by the Guo group.[61−63] They have concluded that the dynamic simulations based on the adiabatic potential energy surfaces are insufficient to describe the tunneling reaction particularly when it takes place in the vicinity of the conical intersection. The nonadiabatic dynamic variables such as the geometric phase or diagonal Born−Oppenheimer corrections had to be invoked for the proper explanation of the experiment.[61−63] In this sense, the difference between ZN and WKB in the tunneling probability calculated along the C−C−S−H torsional angle is quite interesting to be noted again (Figure 7). As mentioned above, the ZN tunneling probability almost vanishes at the planar geometry due the absence of the avoided crossing at the conical intersection whereas the WKB method is only influenced by the adiabatic tunneling barrier height, which would bring a large impact on the effective tunneling rates and KIEs calculated in Figure 6. Quite interestingly, the vanishing of the ZN tunneling probability responsible for the node at the planar conical intersection (Figure 7) reminds us of the

https://doi.org/10.1021/acs.jpca.2c05861
J. Phys. Chem. A 2022, 126, 9594−9604

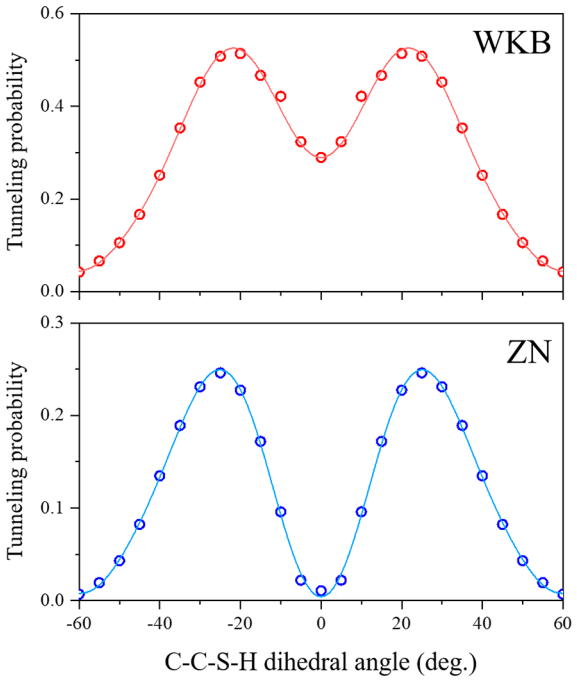

Figure 7. H atom tunneling probability of thiophenol calculated as a function of the C−C−S−H torsional angle by using the WKB approximation (upper trace) or the ZN theory (lower trace). The same two-dimensional potential energy curves have been used for the rate calculations. Note that the ZN theory predicts that the tunneling probability vanishes at the planar configuration where the avoided-crossing rule does not hold due to the presence of the conical intersection. The WKB model is blind to the curve-crossing as it sticks to the adiabatic PES only.

destructive interference of two wavepackets encircling around the conical intersection in the opposite sides due to the geometric phase effect.[73−75] Although the origins of the nodal property of the tunneling probability should be distinct for the semiclassical ZN theory and the full quantum-mechanical calculations, it is notable that the dynamic behaviors at the conical intersection resemble each other.

CONCLUSIONS

Here, the S−H(D) tunneling dissociation dynamics have been interrogated for thiophenol, 2-FTP, 2-MTP, and 2-CTP including their deuterated species. The tunneling rates are semiclassically calculated using the adiabatic WKB method or the nonadiabatic ZN theory based on the one-, two-, or three-dimensional potential energy surfaces in the proximity of the conical intersection to be compared to the state-specifically measured experimental tunneling rates. The dimensional extension of the PES into the C−C−S−H torsional angle coordinate has been found to be most influential on the tunneling dynamics. The adiabatic WKB semiclassical calculations predict the faster tunneling rates whereas the nonadiabatic ZN theory predicts the slower tunneling rates compared to the experimental results. Both WKB and ZN, however, reproduce the experiment within 1 order of magnitude. The KIE on the adiabatic PES in the reduced dimension given in this work is hardly reproduced by the adiabatic WKB model whereas it is relatively well rationalized by the nonadiabatic ZN model, suggesting that the nonadiabatic coupling terms implemented in the latter should play the import role in the tunneling process. The ZN calculation conforms to the geometrical phase effect, impeding the tunneling process through the destructive interference of the wavepackets encircling the conical intersection in the opposite sides. The S−H(D) tunneling predissociation dynamics of the S_1 states of thiophenols (and their deuterated species) presented here provides the nice platform for the thorough investigation of the tunneling reaction taking place in the vicinity of the conical intersection, especially since the tunneling reaction at many outstanding well-identified vibronic modes could be identified prior to the mode randomization to provide the otherwise formidable deep insights into the multidimensionality of the tunneling reaction in terms of the mode-specific rate and kinetic isotope effect. It should be emphasized again that nonadiabatic tunneling dynamics had been thoroughly investigated quantum mechanically using a two state diabatic representation and reduced dimension quantum dynamics for the bare phenol by Xie et al.[61] Accordingly, the quantum mechanical calculations on the nonadiabatic tunneling dynamics of the interesting systems of 2-FTP and 2-MTP presented here would be highly desirable in the near future.

ASSOCIATED CONTENT

Supporting Information

The Supporting Information is available free of charge at https://pubs.acs.org/doi/10.1021/acs.jpca.2c05861.

Computation details, state-specific S_1 lifetime of 2-fluorothiophenol-*d*, one-dimensional potential energy curves along the C−S−H(D) bending coordinate, and one-dimensional potential energy curves along the S−H bond extension coordinate, S_1 lifetimes of thiophenol and thiophenol-*d* at several excitation wavelengths (PDF)

AUTHOR INFORMATION

Corresponding Author

Sang Kyu Kim − *Department of Chemistry, KAIST, Daejeon 34141, Republic of Korea;* orcid.org/0000-0003-4803-1327; Email: sangkyukim@kaist.ac.kr

Authors

Junggil Kim − *Department of Chemistry, KAIST, Daejeon 34141, Republic of Korea*

Kyung Chul Woo − *Department of Chemistry, KAIST, Daejeon 34141, Republic of Korea;* Present Address: Division of Chemistry and Biological Chemistry, School of Physical and Mathematical Sciences, Nanyang Technological University, 637371, Singapore

Kuk Ki Kim − *Department of Chemistry, KAIST, Daejeon 34141, Republic of Korea*

Complete contact information is available at: https://pubs.acs.org/10.1021/acs.jpca.2c05861

Notes

The authors declare no competing financial interest.

ACKNOWLEDGMENTS

Authors greatly appreciate the experimental assistance of and helpful discussion with Dr. Do Hyung Kang and Mr. Minseok Kang. This work was financially supported by the National Research Foundation of Korea (2018R1A2B3004534, 2019K1A3A1A14064258, and 2019R1A6A1A10073887).

REFERENCES

(1) Yarkony, D. R. Conical intersections: Diabolical and often misunderstood. *Acc. Chem. Res.* **1998**, *31*, 511−518.
(2) Yarkony, D. R. Nuclear dynamics near conical intersections in the adiabatic representation: I. The effects of local topography on interstate transitions. *J. Chem. Phys.* **2001**, *114*, 2601.
(3) Tully, J. C. Perspective: Nonadiabatic dynamics theory. *J. Chem. Phys.* **2012**, *137*, 22A301.
(4) Malhado, J. P.; Bearpark, M. J.; Hynes, J. T. Non-adiabatic dynamics close to conical intersections and the surface hopping perspective. *Front. Chem.* **2014**, *2*, 97.
(5) Sobolewski, A. L.; Domcke, W.; Dedonder-Lardeux, C.; Jouvet, C. Excited-state hydrogen detachment and hydrogen transfer driven by repulsive $^1\pi\sigma^*$ states: A new paradigm for nonradiative decay in aromatic biomolecules. *Phys. Chem. Chem. Phys.* **2002**, *4*, 1093−1100.
(6) Ashfold, M. N. R.; King, G. A.; Murdock, D.; Nix, M. G. D.; Oliver, T. A. A.; Sage, A. G. $\pi\sigma^*$ excited states in molecular photochemistry. *Phys. Chem. Chem. Phys.* **2010**, *12*, 1218−1238.
(7) Roberts, G. M.; Stavros, V. G. The role of $\pi\sigma^*$ states in the photochemistry of heteroaromatic biomolecules and their subunits: Insights from gas-phase femtosecond spectroscopy. *Chem. Sci.* **2014**, *5*, 1698−1722.
(8) You, H. S.; Han, S.; Yoon, J.-H.; Lim, J. S.; Lee, J.; Kim, S.-Y.; Ahn, D.-S.; Lim, J. S.; Kim, S. K. Structure and dynamic role of conical intersections in the $\pi\sigma^*$-mediated photodissociation reactions. *Int. Rev. Phys. Chem.* **2015**, *34*, 429−459.
(9) Kim, J.; Woo, K. C.; Kim, K. K.; Kang, M.; Kim, S. K. Tunneling dynamics dictated by the multidimensional conical intersection seam in the $\pi\sigma^*$-mediated photochemistry of heteroaromatic molecules. *Bull. Korean Chem. Soc.* **2022**, *43*, 150−164.
(10) Schoenlein, R. W.; Peteanu, L. A.; Mathies, R. A.; Shank, C. V. The first step in vision: Femtosecond isomerization of rhodopsin. *Science* **1991**, *254*, 412−415.
(11) Satzger, H.; Townsend, D.; Zgierski, M. Z.; Patchkovskii, S.; Ullrich, S.; Stolow, A. Primary processes underlying the photostability of isolated DNA bases: Adenine. *Proc. Natl. Acad. Sci. U. S. A.* **2006**, *103*, 10196−10201.
(12) Asturiol, D.; Lasorne, B.; Worth, G. A.; Robb, M. A.; Blancafort, L. Exploring the sloped-to-peaked S_2/S_1 seam of intersection of thymine with electronic structure and direct quantum dynamics calculations. *Phys. Chem. Chem. Phys.* **2010**, *12*, 4949−4958.
(13) Soorkia, S.; Jouvet, C.; Grégoire, G. UV photoinduced dynamics of conformer-resolved aromatic peptides. *Chem. Rev.* **2020**, *120*, 3296−3327.
(14) Jouvet, C.; Miyazaki, M.; Fujii, M. Revealing the role of excited state proton transfer (ESPT) in excited state hydrogen transfer (ESHT): Systematic study in phenol-$(NH_3)_n$ clusters. *Chem. Sci.* **2021**, *12*, 3836−3856.
(15) Lim, J. S.; Kim, S. K. Experimental probing of conical intersection dynamics in the photodissociation of thioanisole. *Nat. Chem.* **2010**, *2*, 627−632.
(16) Roberts, G. M.; Hadden, D. J.; Bergendahl, L. T.; Wenge, A. M.; Harris, S. J.; Karsili, T. N. V.; Ashfold, M. N. R.; Paterson, M. J.; Stavros, V. G. Exploring quantum phenomena and vibrational control in σ^* mediated photochemistry. *Chem. Sci.* **2013**, *4*, 993−1001.
(17) Han, S.; Lim, J. S.; Yoon, J.-H.; Lee, J.; Kim, S.-Y.; Kim, S. K. Conical intersection seam and bound resonances embedded in continuum observed in the photodissociation of thioanisole-d_3. *J. Chem. Phys.* **2014**, *140*, 054307.
(18) Woo, K. C.; Kang, D. H.; Kim, S. K. Real-time observation of nonadiabatic bifurcation dynamics at a conical intersection. *J. Am. Chem. Soc.* **2017**, *139*, 17152−17158.
(19) Li, S. L.; Truhlar, D. G. Full-dimensional multi-state simulation of the photodissociation of thioanisole. *J. Chem. Phys.* **2017**, *147*, 044311.
(20) Lim, J. S.; You, H. S.; Kim, S.-Y.; Kim, S. K. Experimental observation of nonadiabatic bifurcation dynamics at resonances in the continuum. *Chem. Sci.* **2019**, *10*, 2404−2412.
(21) Lee, H.; Kim, S.-Y.; Kim, S. K. Multidimensional characterization of the conical intersection seam in the normal mode space. *Chem. Sci.* **2020**, *11*, 6856−6861.
(22) Kim, J. B.; Yacovitch, T. I.; Hock, C.; Neumark, D. M. Slow photoelectron velocity-map imaging spectroscopy of the phenoxide and thiophenoxide anions. *Phys. Chem. Chem. Phys.* **2011**, *13*, 17378−17383.
(23) Herzberg, G.; Longuet-Higgins, H. C. Intersection of potential energy surfaces in polyatomic molecules. *Discuss. Faraday Soc.* **1963**, *35*, 77−82.
(24) Herzberg, G.*Electronic spectra and electronic structure of polyatomic molecules*; Van Nostrand: New York, 1966.
(25) Schinke, R.*Photodissociation dynamics: Spectroscopy and fragmentation of small polyatomic molecules*; Cambridge University Press: Cambridge, 1993.
(26) Hoshino-Nagasaka, M.; Suzuki, T.; Ichimura, T.; Kasahara, S.; Baba, M.; Kawauchi, S. Rotationally resolved high-resolution spectrum of the S_1- S_0 transition of jet-cooled thioanisole. *Phys. Chem. Chem. Phys.* **2010**, *12*, 13243−13247.
(27) Devine, A. L.; Nix, M. G. D.; Dixon, R. N.; Ashfold, M. N. R. Near-ultraviolet photodissociation of thiophenol. *J. Phys. Chem. A* **2008**, *112*, 9563−9574.
(28) You, H. S.; Han, S.; Lim, J. S.; Kim, S. K. $(\pi\pi^*/\pi\sigma^*)$ conical intersection seam experimentally observed in the S-D bond dissociation reaction of thiophenol-d_1. *J. Phys. Chem. Lett.* **2015**, *6*, 3202−3208.
(29) Ovejas, V.; Fernández-Fernández, M.; Montero, R.; Longarte, A. On the ultrashort lifetime of electronically excited thiophenol. *Chem. Phys. Lett.* **2016**, *661*, 206−209.
(30) Lin, G.-S.-M.; Xie, C.; Xie, D. Nonadiabatic effect in photodissociation dynamics of thiophenol via the $^1\pi\pi^*$ state. *J. Phys. Chem. A* **2018**, *122*, 5375−5382.
(31) Lim, J. S.; You, H. S.; Han, S.; Kim, S. K. Photodissociation dynamics of ortho-substituted thiophenols at 243 nm. *J. Phys. Chem. A* **2019**, *123*, 2634−2639.
(32) Woo, K. C.; Kim, S. K. Real-time tunneling dynamics through adiabatic potential energy surfaces shaped by a conical intersection. *J. Phys. Chem. Lett.* **2020**, *11*, 6730−6736.
(33) Pino, G. A.; Oldani, A. N.; Marceca, E.; Fujii, M.; Ishiuchi, S.-I.; Miyazaki, M.; Broquier, M.; Dedonder, C.; Jouvet, C. Excited state hydrogen transfer dynamics in substituted phenols and their complexes with ammonia: $\pi\pi^*$-$\pi\sigma^*$ energy gap propensity and *ortho*-substitution effect. *J. Chem. Phys.* **2010**, *133*, 124313.
(34) Roberts, G. M.; Chatterley, A. S.; Young, J. D.; Stavros, V. G. Direct observation of hydrogen tunneling dynamics in photoexcited phenol. *J. Phys. Chem. Lett.* **2012**, *3*, 348−352.
(35) Lai, H. Y.; Jhang, W. R.; Tseng, C.-M. Communication: Mode-dependent excited-state lifetime of phenol under the S_1/S_2 conical intersection. *J. Chem. Phys.* **2018**, *149*, 031104.
(36) Woo, K. C.; Kim, S. K. Multidimensional H atom tunneling dynamics of phenol: Interplay between vibrations and tunneling. *J. Phys. Chem. A* **2019**, *123*, 1529−1537.
(37) Weiler, M.; Miyazaki, M.; Féraud, G.; Ishiuchi, S.; Dedonder, C.; Jouvet, C.; Fujii, M. Unusual behavior in the first excited state lifetime of catechol. *J. Phys. Chem. Lett.* **2013**, *4*, 3819−3823.
(38) Xu, X.; Zheng, J.; Yang, K. R.; Truhlar, D. G. Photodissociation dynamics of phenol: Multistate trajectory simulations including tunneling. *J. Am. Chem. Soc.* **2014**, *136*, 16378−16386.
(39) Woo, K. C.; Kim, J.; Kim, S. K. Conformer-specific tunneling dynamics dictated by the seam coordinate of the conical intersection. *J. Phys. Chem. Lett.* **2021**, *12*, 1854−1861.
(40) Kim, K. K.; Kim, J.; Woo, K. C.; Kim, S. K. S_1-state decay dynamics of benzenediols (catechol, resorcinol, and hydroquinone) and their 1:1 water clusters. *J. Phys. Chem. A* **2021**, *125*, 7655−7661.
(41) Han, S.; You, H. S.; Kim, S.-Y.; Kim, S. K. Dynamic role of the intramolecular hydrogen bonding in nonadiabatic chemistry revealed in the UV photodissociation reactions of 2-fluorothiophenol and 2-chlorothiophenol. *J. Phys. Chem. A* **2014**, *118*, 6940−6949.

https://doi.org/10.1021/acs.jpca.2c05861
J. Phys. Chem. A 2022, 126, 9594−9604

(42) Lim, J. S.; You, H. S.; Kim, S.-Y.; Kim, J.; Park, Y. C.; Kim, S. K. Vibronic structure and predissociation dynamics of 2-methoxythiophenol (S_1): The effect of intramolecular hydrogen bonding on nonadiabatic dynamics. *J. Chem. Phys.* **2019**, *151*, 244305.
(43) Kim, J.; Lim, J. S.; Noh, H.-R.; Kim, S. K. Experimental observation of the Autler-Townes splitting in polyatomic molecules. *J. Phys. Chem. Lett.* **2020**, *11*, 6791−6795.
(44) Lin, G.-S.-M.; Xie, C.; Xie, D. Three-dimensional diabatic potential energy surfaces for the photodissociation of thiophenol. *J. Phys. Chem. A* **2017**, *121*, 8432−8439.
(45) Eppink, A. T. J. B.; Parker, D. H. Velocity map imaging of ions and electrons using electrostatic lenses: Application in photoelectron and photofragment ion imaging of molecular oxygen. *Rev. Sci. Instrum.* **1997**, *68*, 3477.
(46) Werner, H.-J.; Knowles, P. J.; Knizia, G.; Manby, F. R.; Schütz, M. Molpro: A general-purpose quantum chemistry program package. *Wiley Interdiscip. Rev.: Comput. Mol. Sci.* **2012**, *2*, 242−253.
(47) Venkatesan, T. S.; Ramesh, S. G.; Lan, Z.; Domcke, W. Theoretical analysis of photoinduced H-atom elimination in thiophenol. *J. Chem. Phys.* **2012**, *136*, 174312.
(48) Zhang, L.; Truhlar, D. G.; Sun, S. Full-dimensional three-state potential energy surfaces and state couplings for photodissociation of thiophenol. *J. Chem. Phys.* **2019**, *151*, 154306.
(49) Yamamoto, S.; Ebata, T.; Ito, M. Rotational isomers of *o*-chlorophenol and their different emission properties. *J. Phys. Chem.* **1989**, *93*, 6340−6345.
(50) Harris, S. J.; Karsili, T. N. V.; Murdock, D.; Oliver, T. A. A.; Wenge, A. M.; Zaouris, D. K.; Ashfold, M. N. R.; Harvey, J. N.; Few, J. D.; Gowrie, S.; et al. A multipronged comparative study of the ultraviolet photochemistry of 2-, 3-, and 4-chlorophenol in the gas phase. *J. Phys. Chem. A* **2015**, *119*, 6045−6056.
(51) Deng, X.; Tang, Y.; Song, X.; Liu, K.; Gu, Z.; Zhang, B. Photolysis dynamics of m- and o-fluorophenol: Substitution effects on tunneling mechanism. *Chemosphere* **2020**, *253*, 126747.
(52) Marston, C. C.; Balint-Kurti, G. G. The Fourier grid Hamiltonian method for bound state eigenvalues and eigenfunctions. *J. Chem. Phys.* **1989**, *91*, 3571.
(53) Zhu, C.; Nakamura, H. The two-state linear curve crossing problems revisited. III. Analytical approximations for Stokes constant and scattering matrix: Nonadiabatic tunneling case. *J. Chem. Phys.* **1993**, *98*, 6208.
(54) Zhu, C.; Nakamura, H. Theory of nonadiabatic transition for general two-state curve crossing problems. I. Nonadiabatic tunneling case. *J. Chem. Phys.* **1994**, *101*, 10630.
(55) Zhu, C.; Nakamura, H. Usefulness of the newly completed semiclassical theory for curve crossing: Multi-channel resonant scattering. *Chem. Phys. Lett.* **1997**, *274*, 205−212.
(56) Ishida, T.; Nanbu, S.; Nakamura, H. Clarification of nonadiabatic chemical dynamics by the Zhu-Nakamura theory of nonadiabatic transition: From tri-atomic systems to reactions in solutions. *Int. Rev. Phys. Chem.* **2017**, *36*, 229−285.
(57) Gao, A.-H.; Li, B.; Zhang, P.-Y.; Han, K.-L. Nonadiabatic *ab initio* molecular dynamics of photoisomerization in bridged azobenzene. *J. Chem. Phys.* **2012**, *137*, 204305.
(58) Xu, C.; Yu, L.; Zhu, C.; Yu, J.; Cao, Z. Intersystem crossing-branched excited-state intramolecular proton transfer for o-nitrophenol: An ab initio on-the-fly nonadiabatic molecular dynamic simulation. *Sci. Rep.* **2016**, *6*, 26768.
(59) Yue, L.; Yu, L.; Xu, C.; Lei, Y.; Liu, Y.; Zhu, C. Benchmark performance of global switching versus local switching for trajectory surface hopping molecular dynamics simulation: *Cis*↔*trans* azobenzene photoisomerization. *ChemPhysChem.* **2017**, *18*, 1274−1287.
(60) Gao, A.; Wang, M.; Ding, J. Ultrafast *trans-cis* photoisomerization of the neutral chromophore in green fluorsecent proteins: Surface-hopping dynamics simulation. *J. Chem. Phys.* **2018**, *149*, 074304.
(61) Xie, C.; Ma, J.; Zhu, X.; Yarkony, D. R.; Xie, D.; Guo, H. Nonadiabatic tunneling in photodissociation of phenol. *J. Am. Chem. Soc.* **2016**, *138*, 7828−7831.
(62) Xie, C.; Yarkony, D. R.; Guo, H. Nonadiabatic tunneling via conical intersections and the role of the geometric phase. *Phys. Rev. A* **2017**, *95*, 022104.
(63) Xie, C.; Kendrick, B. K.; Yarkony, D. R.; Guo, H. Constructive and destructive interference in nonadiabatic tunneling via conical intersections. *J. Chem. Theory Comput.* **2017**, *13*, 1902−1910.
(64) Miller, S. C., Jr.; Good, R. H., Jr. A WKB-type approximation to the Schrödinger equation. *Phys. Rev.* **1953**, *91*, 174.
(65) Quanz, H.; Schreiner, P. R. TUNNEX: An easy-to-use Wentzel-Kramers-Brillouin (WKB) implementation to compute tunneling half-lives. *J. Comput. Chem.* **2019**, *40*, 543−547.
(66) Kuznetsov, A. M.; Ulstrup, J. Proton and hydrogen atom tunnelling in hydrolytic and redox enzyme catalysis. *Can. J. Chem.* **1999**, *77*, 1085−1096.
(67) Costentin, C.; Robert, M.; Savéant, J.-M.; Tard, C. Inserting a hydrogen-bond relay between proton exchanging sites in proton-coupled electron transfer. *Angew. Chem., Int. Ed.* **2010**, *49*, 3803−3806.
(68) Costentin, C.; Robert, M.; Savéant, J.-M. Concerted proton-electron transfer in the oxidation of phenols. *Phys. Chem. Chem. Phys.* **2010**, *12*, 11179−11190.
(69) Benabbas, A.; Salna, B.; Sage, J. T.; Champion, P. M. Deep proton tunneling in the electronically adiabatic and non-adiabatic limits: Comparison of the quantum and classical treatment of donor-acceptor motion in a protein environment. *J. Chem. Phys.* **2015**, *142*, 114101.
(70) Klinman, J. P.; Offenbacher, A. R.; Hu, S. Origins of enzyme catalysis: Experimental findings for C-H activation, new models, and their relevance to prevailing theoretical constructs. *J. Am. Chem. Soc.* **2017**, *139*, 18409−18427.
(71) Sakaushi, K.; Kumeda, T.; Hammes-Schiffer, S.; Melander, M. M.; Sugino, O. Advances and challenges for experiment and theory for multi-electron multi-proton transfer at electrified solid-liquid interfaces. *Phys. Chem. Chem. Phys.* **2020**, *22*, 19401−19442.
(72) Liu, Y.; Yan, Y.; Xing, T.; Shi, Q. Understanding the large kinetic isotope effect of hydrogen tunneling in condensed phases by using double-well model systems. *J. Phys. Chem. B* **2021**, *125*, 5959−5970.
(73) Mead, C. A.; Truhlar, D. G. On the determination of Born-Oppenheimer nuclear motion wave functions including complications due to conical intersections and identical nuclei. *J. Chem. Phys.* **1979**, *70*, 2284.
(74) Berry, M. V. Quantal phase factors accompanying adiabatic changes. *Proc. R. Soc. London A* **1984**, *392*, 45−57.
(75) Mead, C. A. The geometric phase in molecular systems. *Rev. Mod. Phys.* **1992**, *64*, 51−85.

https://doi.org/10.1021/acs.jpca.2c05861
J. Phys. Chem. A 2022, 126, 9594−9604